

The relationship between wind speed and precipitation
in the Pacific ITCZ

Larissa E. Back*

Department of Atmospheric Sciences

University of Washington, Seattle, WA

Christopher S. Bretherton

Department of Atmospheric Sciences

University of Washington, Seattle, WA

Submitted to *J. Climate*, 13 Oct 2004, revised 3 March 2005

*Full address: Department of Atmospheric Sciences, University of Washington, Box 351640, Seattle, WA 98195-1640. E-mail: larissa@atmos.washington.edu

Abstract

The relationship between wind speed and precipitation in the Pacific ITCZ is analyzed using four years of daily SSM/I and TMI satellite passive microwave retrievals averaged over $2\ 1/2$ degree boxes. Throughout the ITCZ, at high column relative humidities (conditions under which deep convection is likely to occur), faster winds are associated with substantially more precipitation, explaining a small, but highly statistically significant fraction of daily rainfall variability. The slope of this relationship varies geographically and rapidly increases as the atmosphere becomes moister. Analysis of other data sources, including vector mean winds computed from QuikSCAT and area-averaged radar-derived precipitation estimates from Kwajalein Island, shows that the wind speed-precipitation correlation is robust.

This relation provides a test of large-scale forecast models and insight into conceptual models of deep convection. The observed increases in precipitation are much greater than evaporation changes associated with the increased wind speed, this implies a convergence feedback by which evaporation induces moisture convergence that feeds increases in precipitation. The authors study whether ERA40 and NCEP reanalyses show the observed wind speed-precipitation correlation and explore mechanisms for convergence feedback using column-integrated moist static energy budgets computed from the reanalyses.

1 Introduction

Over the tropical oceans, averaged over a region several hundred kilometers on a side, evaporation is expected to be roughly proportional to wind speed because near-surface humidity and temperature are relatively uniform, even as wind speed and area-averaged precipitation rate fluctuate greatly from day to day (Raymond et al. 2003, Sobel et al. 2004, Johnson and Lin 1997, Bretherton et al. 2004). Higher wind speeds are associated with more evaporation and latent heat flux from the ocean to the atmosphere. In regions of persistent deep tropical convection, it has been suggested that “convection follows the winds,” i.e. in a region and period of increased mean surface winds, rainfall is enhanced due to increased surface latent heat fluxes (Raymond et al. 2003). In the East Pacific, using dropsonde data taken during the Eastern Pacific Investigation of Climate (EPIC), Raymond et al. (2003) found that day to day variations in surface entropy fluxes (mainly associated with evaporation) computed from dropsonde measurements and averaged over a 400×400 km region were highly correlated with precipitation. However, this idea has never been tested using a large observational dataset, like that provided by passive microwave sensor satellite retrievals of wind speed and precipitation. In this paper, we look for relationships between area-averaged, satellite-derived wind speed and precipitation throughout the Pacific Intertropical Convergence Zone (ITCZ) and compare our findings to some simple conceptual models of tropical oceanic convection and its relationship to large-scale circulations.

Many convective closures utilize the idea of a statistical ‘quasi-equilibrium’ on larger-than-convective (but still sub-daily) timescales, between the large-scale processes that pro-

mote convective instability and the instability being removed by convection (e.g. Arakawa and Schubert 1974, Raymond 1995). Other 'moist adjustment' schemes relax the atmospheric temperature and moisture profiles to specified vertical structures when convective instability is diagnosed (e.g. Betts and Miller 1986). In either case, we anticipate that in regions of persistent convection there will likely be statistical correlations between 'forcings' such as evaporative moistening of the planetary boundary layer (PBL) and rainfall. These correlations can provide useful insights into the convective dynamics and serve as useful tests for large-scale models and their embedded convective parameterizations.

Evaporation alone introduces little water when compared to the daily precipitation amounts typically observed in mesoscale convective complexes. Instead, the main immediate moisture source for the precipitation is moisture convergence. This suggests that a "convergence feedback" is occurring, in which small increases in evaporation drive much larger increases in moisture convergence and precipitation.

Here, we use four years of passive microwave satellite data to test daily wind speed-precipitation correlations in the Pacific ITCZ. To test the robustness of the wind speed-precipitation correlation, we also use several months of ground-based radar-derived area-averaged precipitation measurements from Kwajalein Island in the central Pacific ITCZ, as well as vector wind retrievals from QuikSCAT. Then we investigate whether data from two reanalyses captures the observed wind speed-precipitation correlation: the European Center for Medium-Range Weather Forecasts (ECMWF) 40-year reanalysis (ERA40) and the National Centers for Environmental Prediction (NCEP) reanalysis. The reanalysis data

is then further used to explore possible mechanisms for convergence feedback, using column-integrated moist static energy budgets.

2 Data description

We use a methodology similar to that used by Bretherton et al. (2004), hereafter BPB04, who describe simple relationships between humidity and precipitation over tropical ocean regions. As in BPB04, we obtained 0.25° gridded retrievals (retrieval algorithm version 5.0) of precipitation, water vapor path, and surface wind speed (normalized to 10 meters) from Remote Sensing Systems (URL: <http://www.ssmi.com>) for all satellite passes of the Special Sensor Microwave/Imager (SSM/I) and TRMM Microwave Imager (TMI) that occurred during 1998 through 2001. The retrieval algorithm, described in detail in Wentz and Spencer (1998), uses brightness temperatures observed at 19.35, 22.235, 37 and 85 GHz to simultaneously estimate rain rate, water vapor path, near-surface wind speed and cloud liquid water. For the analysis, the gridded data was first averaged over all available passes (typically 2-6), each day at each grid column, and then averaged to a coarser 2.5° grid, as described in BPB04. To maintain consistency with SSM/I retrievals, a potentially more accurate wind speed estimate for TMI overpasses that also uses the TMI 11 GHz channel was not used; instead the Wentz algorithm based on the 37 GHz channel for wind speed retrieval was used for both TMI and SSM/I. No correction was made to account for possible biases associated with uneven sampling of the diurnal cycle. For validation of the SSM/I wind speeds, we use QuikSCAT SeaWinds gridded, daily vector wind retrievals, also obtained from Remote

Sensing Systems.

From the Data Support Section of the National Center for Atmospheric Research (NCAR), we obtained ECMWF 40 year reanalysis (ERA40, 23 pressure levels, 2.5° grid, URL: <http://www.ecmwf.int>), temperature, wind speeds, humidity, precipitation, surface latent and sensible heat fluxes, and net radiative fluxes at the surface and top of atmosphere. From the Climate Diagnostics Center (URL: <http://www.cdc.noaa.gov>), we also obtained comparable NCEP reanalysis data (17 pressure levels, 2.5° grid, Kalnay et al. 1996). From reanalysis temperatures, we computed daily average saturation water vapor path at each point following BPB04.

3 Microwave-derived relationships between precipitation and wind speed

We examined the relationship between $5^\circ \times 5^\circ$ daily averaged wind speed and precipitation (from the SSM/I and TMI) at 10°N at several longitudes which are in the Pacific ITCZ for much of the year. First, four adjacent $2.5^\circ \times 2.5^\circ$ gridpoints were averaged into a $550 \text{ km} \times 550 \text{ km}$ box at each longitude. Then all four years of wind speed and precipitation data (1461 days) were sorted by wind speed and subdivided into bins containing 60 gridpoint-days of data (24 bins at each location). Within each such bin, the mean, 25th, 50th and 75th percentiles of the 60 precipitation estimates were calculated. $5^\circ \times 5^\circ$ boxes were used instead of $2.5^\circ \times 2.5^\circ$ boxes to average out some of the random measurement error in the SSM/I precipitation retrievals, but our results are not sensitive to this choice. Fig. 1 illustrates

this analysis in the western Pacific warm pool (at 160°E, 10°N), and in the eastern Pacific ITCZ (at 95°W, 10°N). In the western Pacific warm pool (Fig. 1a) no relationship between wind speed and rainfall is visible. However, in the eastern Pacific (Fig. 1b) there tends to be more rainfall on days with stronger winds. The correlation coefficient of daily wind speed with daily rainfall is 0.32, which is highly statistically significant. The sample size of 1461 corresponds to 570 degrees of freedom (taking into account the lag-one autocorrelation in time), so a correlation coefficient of 0.05 is statistically significant at the 99.95 percent level. However, on many high wind speed days there is no precipitation.

A complicating factor in this analysis is that the precipitation belts vary with the seasonal cycle. Only when convection is easily and frequently initiated do we expect to see a correlation between wind speed and precipitation. Outside deep convective regions, high wind speeds still enhance surface moisture fluxes, but this moisture is stored and advected downstream rather than being rained out locally. BPB04 found that “column relative humidity” r , defined as water vapor path (WVP) divided by saturation WVP is strongly correlated with daily precipitation. When r is low, it does not rain, even when winds are strong. A single exponential fit curve, with near-doubling of expected precipitation for each 4 percent increase in r , is adequate to describe the SSM/I-derived r -precipitation correlation in all tropical ocean regions.

To control for these seasonal variations at each location, we repeated the analysis of Fig. 1, isolating only those days in the four-year record with r greater than 0.75, to focus only on those times when it is likely to rain. From Fig. 4 of BPB04, at $r = 0.75$, the

25th, 50th and 75th percentiles of SSM/I-derived rainfall are 2, 5 and 12 mm d⁻¹; the true rainfall distribution at this r is likely more narrowly peaked (BPB04) and nearly excludes non-raining days. Fig. 2 shows that with this r threshold, there is a remarkable linear correlation between wind speed and precipitation at all ITCZ locations examined. As in Fig. 1, at each location the wind speed and precipitation data was sorted by wind speed and subdivided into bins of 60 gridpoint-days. On days with stronger winds there tends to be more rainfall. Even in the eastern Pacific, the correlation is substantially stronger than in Fig. 1, and the quartiles plotted show many fewer high wind speed days during which there is no precipitation.

In the ERA40 and NCEP reanalyses, (averaged daily over $2.5^\circ \times 2.5^\circ$ centered on the same locations as the wind speed and precipitation) the increase in evaporation that occurs as wind speed rises from 4 to 8 m s⁻¹ averages less than 3 mm d⁻¹ (over the grid-point days used in 2), small compared with the observed increases in precipitation. This is consistent with a convergence feedback.

Wind speed explains a moderate amount of the daily variability in precipitation, as is visible in the correlation coefficients and quartiles plotted in Fig. 2. The trends are highly statistically significant at all plotted locations due to the large amount of data (266-545 days with $r > 0.75$). A correlation of 0.13 is statistically significant at the 99.95 percent level at all locations (degrees of freedom range from 166 to 460 taking into account the lag-one autocorrelation). The correlation and the regression slope in Fig. 2 vary spatially, with the highest correlation and the steepest slope (greatest increase in precipitation for a given

increase in wind speed) east of 120°W . There is also a strong correlation in the western Pacific (160°W), but the slope is not as steep as in the eastern Pacific. In the central Pacific, the correlations are not as strong, and the slopes are less steep.

One possible explanation for the spatial variations in the wind speed-precipitation relationship is that moisture advection could be varying. Reanalyses (discussed further in Section 6) suggest moisture advection is generally a drying effect in the ITCZ. Thus, increased dry advection in higher wind conditions could counter-balance the increases in evaporation. Another possibility is that the amount of induced moisture convergence could vary in association with the mean thermodynamic and vertical motion profiles. In Section 6, we will investigate these ideas using reanalysis data.

3.1 Relationship to QuikSCAT vector mean winds

Since the passive microwave imagers (SSM/I and TMI) do not measure wind direction, and wind speeds have been spatially averaged to 2.5° resolution from 0.25° resolution, the correlation of wind speed with precipitation could be due to mean wind speed enhancement around heavily precipitating mesoscale convective systems. By looking at vector mean winds over a 2.5° grid instead of mean wind speeds, we can test this idea since mesoscale gustiness should contribute little to the vector mean winds even where it increases the mean wind speed. The passive microwave imagers retrieve wind speed based on surface roughness, so opposing winds within a grid-point day will not average out to zero; this is not the case when high-resolution vector winds are averaged.

We obtained 0.25° gridded QuikSCAT SeaWinds vector winds (June 1999- Dec 2001) from the Physical Oceanography Distributed Active Archive Center (PO.DAAC) at the NASA Jet Propulsion Laboratory (URL: <http://podaac.jpl.nasa.gov>) and calculated $2.5^\circ \times 2.5^\circ$ daily vector mean winds using the ascending and descending passes. Each 2.5° gridpoint-day is thus a composite of between 1 and 2 satellite passes, so these daily QuikSCAT winds include substantially fewer samples than the daily passive microwave winds. To compare the QuikSCAT vector mean winds to the SSM/I and TMI wind speeds, Fig. 3a shows a representative example from 95°W of the QuikSCAT daily vector mean winds (vector mean wind speed of four 2.5° gridpoints averaged together) binned against the passive microwave winds in the Pacific ITCZ. The correlation coefficient of 0.87 is very high. The microwave-derived wind speeds are consistently stronger than vector mean winds inferred from QuikSCAT, especially at higher wind speeds. This difference in wind strength (robust to various methods of determining slope) is presumably due to a combination of systematic errors, convective gustiness and sampling differences.

The microwave imager-derived daily precipitation on r -thresholded days was also binned against the QuikSCAT daily vector mean winds. An example from the 95°W , 10°N point is shown in Fig. 3b. The correlation is qualitatively similar to that in Fig. 2, which suggests that the enhanced precipitation variability is associated with sustained strong vector-mean wind conditions, rather than precipitation creating a wind speed-rainfall correlation by inducing enhanced mesoscale gustiness.

3.2 Dependence on column relative humidity

It is natural to ask whether the relationship between water vapor path and precipitation described by BPB04 and our relationship between wind speed and precipitation are independent effects. To answer this question, we looked at the dependence of the SSM/I and TMI-derived wind speed-precipitation correlation on column relative humidity. All data, averaged to $5^\circ \times 5^\circ$ boxes, from the longitudes in the region along 10°N where the wind speed-precipitation correlation was strongest (125°W to 85°W), were subdivided into column relative humidity bins. Within each humidity category, the precipitation measurements were binned by wind speed. Fig. 4 shows the distribution of precipitation as a function of wind speed for several column relative humidity (r) categories, using both SSM/I-TMI wind speeds and QuikSCAT vector mean winds. In each column relative humidity category there is a linear increase of precipitation with wind speed. In more humid conditions, the increase in precipitation associated with increasing wind speed is greater.

4 Validation using KWAJEX data

There are a number of uncertainties involved in the retrieval of precipitation estimates from the SSM/I on a daily timescale. Inherent in the empirical Wentz algorithm are random errors in retrieving precipitation associated with ambiguities in mapping brightness temperature to rainfall. There are errors associated with horizontally inhomogeneous precipitation being treated as uniform on retrieval scales, even though there is a non-linear relationship between brightness temperature and precipitation. Even if retrievals were perfect, convection evolves

over the course of a day and one may ask whether 2-6 retrievals averaged over a 5 degree box are an adequate sample.

To address these concerns, BPB04 describe a detailed comparison between the daily SSM/I data and an 18 month sample (July-December 1999-2001) of a Kwajalein radar-derived estimate of daily rainfall area-averaged over a circle of 240km radius. The SSM/I wind speed data and the column relative humidity data were averaged over the two closest $2.5^\circ \times 2.5^\circ$ grid boxes to Kwajalein (8.72°N , 167.73°E), centered at 8.75°N , 168.75°W and 8.75°N , 166.25°W .

We calculated the distribution of this Kwajalein radar-derived rainfall proxy, binned by wind speed, for days when column relative humidity is above 0.75 (shown in Fig. 5a, 5c). The correlation of QuikSCAT vector mean winds with the radar rainfall proxy (Fig. 5c) is similar to the wind-precipitation relationship derived using only the passive microwave imagers (Fig. 5b). A correlation coefficient of 0.12 is statistically significant at the 99 percent level given the sample size (270 days, 180 degrees of freedom). The weaker relationship between the QuikSCAT vector mean winds and the SSM/I-TMI precipitation (Fig. 5d) may be due to a combination of the smaller sample size (as mentioned above, only 1 - 2 QuikSCAT satellite passes occur each day compared to 2-6 passive microwave passes) and non-concurrent sampling by the two satellites. Fig. 5 supports the nature of the passive microwave-derived relationships between wind speed and precipitation. A natural extension of this work would be to perform a similar analysis using the TRMM Precipitation Radar combined with simultaneous TMI-derived wind speeds and column relative humidity.

5 Comparison of passive microwave wind speed-precipitation correlation with reanalyses

A remaining question is whether the documented wind speed-precipitation correlation is a feature that is generally captured in ERA40 and NCEP reanalyses and if so, whether the reanalyses can help us better understand it. We first test the extent to which these reanalyses reproduce the observed correlation between wind speed and precipitation at high column relative humidity r .

ERA40 water vapor path is very closely correlated (correlation coefficient 0.95 using 1998-2001 data in Pacific at 10° N) with SSM/I-TMI retrievals (from which ERA40 assimilates retrievals of WVP and wind speed) but ERA40 has substantially more high r occurrences than are observed. NCEP WVP is less strongly correlated (correlation coefficient 0.70) with the SSM/I-TMI product (which NCEP does not assimilate) and r tends to be lower than observed. Although ERA40 has a wider range of column relative humidities and more precipitation than NCEP, both reanalyses have similar relationships between r and precipitation, which are qualitatively, but not quantitatively similar to the SSM/I-derived relationship (not shown).

Since the two reanalyses have similar r -precipitation relationships, we test for a wind speed-precipitation correlation as in Fig. 4. Typical examples from NCEP and ERA40 of the distribution of precipitation binned by wind speed on days with $r \approx 0.75$ are shown in Fig 6. ERA40 has a only a very weak correlation between wind speed and precipitation in the

Eastern Pacific (Fig. 6a) though the correlation is higher in the Western Pacific (correlation coefficient 0.40). This is somewhat surprising since ERA40 assimilates both the SSM/I-TMI water vapor path and wind speed. ERA40 and SSM/I wind speed only have a correlation coefficient of 0.60, so the SSM/I wind speed is clearly used only as a weak constraint on the ERA40. NCEP does not assimilate the SSM/I-TMI data, but the NCEP reanalysis shows a stronger, more consistent wind speed-precipitation correlation (Fig. 6b) when binned by r . The discrepancies in the wind speed-precipitation relationship between observations and the two reanalyses suggest that this relationship is a useful test of the parameterization of moist convective processes in large-scale models.

6 Interpretation of wind speed-precipitation correlation

In this section, we proceed from the hypothesis that the observed wind speed-precipitation correlation is the result of a convergence feedback in which small evaporation anomalies drive larger precipitation anomalies (fed by moisture convergence) and explore possible mechanisms for the convergence feedback.

While the main moisture source for precipitation is moisture convergence, this does not mean moisture convergence should be regarded as a conceptually separate external forcing that “causes” precipitation. Due to vertical moisture stratification in the atmosphere, the horizontal convergence at lower levels and divergence aloft associated with upward motion

naturally induces moisture convergence. Hence, moisture convergence can be viewed as a response to latent heating due to deep convection. Since latent heating occurs as a result of moisture convergence and condensation, this chain of logic is circular. A different framework is required to understand when and where convection occurs within large-scale regions of mean convergence like the ITCZ.

One perspective on the problem is through a column-integrated moist static energy budget (schematic shown in Figure 7). To a first approximation, column moist static energy is not changed by convective circulations within the column itself. Hence, time-mean sources of tropospheric column-integrated moist static energy must be balanced by advective export of moist static energy (Neelin and Held 1987). Two-layer and idealized models of the tropical circulation, (e.g. Neelin and Held 1987, Zebiak 1986, Neelin and Zeng 2000, Sobel and Bretherton 2000) have suggested that evaporation (or more generally, local sources of troposphere-integrated moist static energy) and precipitation (associated with the export of moist static energy) may drive much larger anomalies in precipitation, mainly through a “vertical MSE advection” feedback mechanism. Increased evaporation moistens the PBL, promoting conditional instability and more convection, and adding moist static energy (MSE) to the atmospheric column. The enhanced deep convection diverges the added MSE through divergence of air with higher MSE in the upper troposphere and convergence of air with slightly lower MSE in the lower and mid-troposphere. The enhanced convection also increases moisture convergence, allowing a large precipitation response. In this view, the degree to which convection is enhanced depends on the “gross moist stability,” defined as

the net export of MSE per unit of net upward convective mass flux; a smaller gross moist stability requires more convective enhancement to export a given amount of column MSE. Sobel and Bretherton, however, noted that the relationship between evaporation and precipitation is not convincingly borne out in observations and suggested that horizontal moisture advection might also be playing a role in determining the distribution of precipitation over the warm sea surface temperature regions.

To test the hypothesis that local sources of MSE could enhance convection by causing advective export of MSE by divergent circulations, we computed moist static energy budget terms from ERA40 and the NCEP reanalysis. Although an individual realization of reanalysis data may have substantial errors, we hope that by statistically analyzing the large datasets (4 years of daily data at 2.5° resolution), we can extract some useful information. The reanalyses are subject to possible model biases and have substantially more uncertainty than exists in the observed wind speed-precipitation relationship, but comparison of the two reanalyses may at least suggest a range of plausible values for individual budget terms.

At each pressure level provided to us in each reanalysis, storage, horizontal advection and vertical advection were computed from both reanalyses, corresponding to the first four terms in the budget equation for MSE (h):

$$\frac{dh}{dt} = -\left(u\frac{dh}{dx} + v\frac{dh}{dy} + \omega\frac{dh}{dp}\right) + g\frac{d}{dp}[F_{turb}^h + F_{rad}] + S_h \quad (1)$$

The fifth and sixth terms describe turbulent transport of h and the radiative flux divergence, respectively. S_h includes small source terms due to the nonconservation of h in moist

thermodynamic processes, particularly involving ice. We vertically integrate (1), assuming no top-of-atmosphere turbulent fluxes (brackets indicate mass-weighted vertical integrals of storage, horizontal and vertical advection):

$$\left\langle \frac{dh}{dt} \right\rangle = \left\langle -u \frac{dh}{dx} - v \frac{dh}{dy} \right\rangle + \left\langle -\omega \frac{dh}{dp} \right\rangle + F_{turb}^h(0) + \Delta F_{rad} + R_h \quad (2)$$

We also extracted net column-integrated radiative cooling ΔF_{rad} and surface MSE fluxes $F_{turb}^h(0)$ from the reanalyses. R_h is a residual due to small vertically-averaged source terms $\langle S_h \rangle$, discretization errors due to the limited resolution of the reanalysis output, and mean drifts of the model from reality. If the MSE budget is consistent, R_h should be small compared to the dominant budget terms.

Column-integrated budget terms from (2) were geographically combined, as in Fig. 4, binned by column relative humidity and then within each column relative humidity bin, binned by wind speed with a bin size of 60 gridpoint-days. A caveat to the analysis, as applied to vertical advection, is that model vertical motion is correlated strongly with precipitation, and reanalysis precipitation is not necessarily accurate, or even strongly correlated with wind speed, as Fig. 6a shows. Hence, vertical h advection and its trends with wind speed may be quite inaccurate; we might hope horizontal h advection to be more reliable. For both NCEP and ERA40 budgets, r and wind speed-binned budget residuals R_h are wind speed independent, averaging less than $40 W m^{-1}$ at all wind speeds, and surface heat fluxes are well correlated with wind speed as expected. Storage is also small in the mean and ΔF_{rad} is only weakly wind speed-dependent.

The two reanalyses give surprisingly different estimates of horizontal advection (mainly associated with differences in moisture advection). Fig. 8 shows examples of column-integrated horizontal and vertical advection as well as evaporation as a function of wind speed in the East and West Pacific ITCZ regions we previously analyzed. Column relative humidities in the example shown are approximately 0.75, but the nature of the result is not sensitive to this choice. In the two ERA40 cases, as wind speed increases, horizontal dry advection increases at a similar rate to the evaporation increase (about 10 W m^{-2} per 1 m s^{-1} increase in wind speed). The result of these cancelling effects is that increases in wind speed do not generally feed more moist static energy into the tropospheric column. Thus there is no need for vertical advection to close the MSE budget, and in fact ERA40-predicted vertical advection is comparatively small at all wind speeds.

In the NCEP reanalysis, horizontal advection is a weaker function of wind speed in both regions. In the western Pacific, dry advection is wind speed independent, and vertical advective export of MSE balances the evaporation increases in higher wind speed conditions. In the NCEP east Pacific case, horizontal and vertical advection both contribute roughly equally to balancing the evaporative source. Both NCEP cases are compatible with the vertical MSE advection feedback mechanism, in contrast to ERA40.

Since the ERA40 is incompatible with the vertical MSE advection mechanism for convergence feedback, we also consider two other related mechanisms that do not require column-integrated vertical MSE advection to balance surface fluxes.

Raymond (1995) suggested a related theory for a relationship between evaporation and

rainfall, “boundary layer quasi-equilibrium” (BLQ), where on larger-than-convective timescales, boundary layer MSE remains roughly constant through a balance between evaporative fluxes generating MSE and evaporatively cooled downdrafts from deep convection flushing low MSE air into the boundary layer (Raymond 1995, Raymond et al. 2003). A simple schematic of this theory is shown in Figure 9. In this case, the term “boundary layer” must be extended above cloud base since shallow cumulus circulations are responsible for substantial mixing on these timescales. For the purposes of this paper, we follow Raymond et al. (2003) and view this balanced shallow mixing layer as extending roughly up to 850mb.

As with the vertical MSE advection mechanism, horizontal MSE advection is considered secondary in this balance. A substantial amount of horizontal MSE advection occurs above 850mb, so it is natural to ask whether the evaporative moistening dominates over the dry advection within the boundary layer in both the ERA40 and NCEP reanalyses, even if this is not the case for the whole troposphere. If this were the case, both reanalyses could be consistent with BLQ.

An attraction of the BLQ theory is that it could also explain why the slope of the wind speed-precipitation correlation is greater for higher column relative humidity conditions. The dominant boundary layer MSE source is assumed to be evaporation E , balanced by an MSE sink $M_d\Delta h$, from deep convective low- h downdrafts. MSE storage, horizontal advection and radiation vertically integrated over the boundary layer are considered to be less important. Δh is the typical MSE deficit of downdraft air compared to the boundary layer, and M_d is the downdraft mass flux. M_d is assumed proportional to updraft mass flux M_u which in turn

is proportional to precipitation. Hence the dominant MSE balance in the boundary layer is

$$E = M_d \Delta h = E = cP \Delta h \quad (3)$$

While we do not know the exact behavior of $c = M_d/P$ (the downdraft mass associated with a given amount of precipitation), we expect that in a moister environment, both c and Δh would decrease since there would be less evaporative cooling surrounding updrafts. Hence updraft mass (and precipitation) would need to increase to sustain a given E . This implies P/E larger at high r , as observed.

To test the BLQ theory, we calculated moist static energy budgets (using the reanalyses) for the 850mb to surface layer in each column, and again stratified the data by r and wind speed. BLQ would predict higher wind speeds to consistently be associated with significantly stronger evaporation than horizontal MSE advection in the boundary layer. However, the relationship between wind speed and boundary layer horizontal MSE advection in both the ERA40 and NCEP is similar to the column-integrated horizontal advection shown in Fig. 8. Thus, the boundary layer horizontal MSE advection in NCEP is compatible with BLQ. As in the full tropospheric column, in ERA40, increased low level dry advection occurring at higher wind speeds cancels the evaporation increases, so net boundary layer moistening associated with increases in wind speed is very small. Hence, the ERA40 is not compatible with BLQ.

We propose a third conceptual model for the wind speed-precipitation feedback, which we cannot test using the reanalyses, that is a variation on BLQ. It posits that wind-induced

evaporation increases the shallow cumulus population (Fig. 10). Each shallow cumulus up-draft has a chance of deepening into a precipitating system that depends mainly on ambient humidity. Thus, both stronger winds and increased column relative humidity lead to more precipitation, even if there is no net vertical advection of MSE in the column average or below 850mb. This hypothesis would perhaps best first be tested using simulations with a cloud-resolving model.

7 Conclusion

Four years of passive microwave satellite retrievals from the SSM/I and TMI were used to look at the relationship between daily wind speed and precipitation. At high column relative humidities (conditions under which deep convection is likely to occur) there is a significant correlation between wind speed and precipitation. The slope of the wind speed-precipitation correlation varies geographically, and rapidly increases in moister conditions. Surface wind speed explains a small fraction of the daily rainfall variability, but provides useful insight into how surface forcing modulates tropical convection and also provides an interesting test on large-scale forecast models in the tropics. QuikSCAT data shows the correlation is not associated with mesoscale gustiness induced by convective systems. Hence, the higher surface fluxes are likely causing the incidence of deep convection to increase.

Other data sources were analyzed to show the result is robust. Area-averaged precipitation estimates derived from a radar at Kwajalein Island were compared with the microwave precipitation estimates, and 2.5 degree vector mean winds computed from QuickSCAT were

compared with the SSM/I and TMI-derived wind speeds. In all cases, a wind speed-precipitation correlation is observed in moist conditions.

Physically, higher wind speeds promote more evaporation, which destabilizes the boundary layer and can trigger deep convection. However, quantification of this argument proves unexpectedly subtle. The observed increases in precipitation are much greater than evaporation changes associated with the increased wind speed, so we deduce a convergence feedback is occurring. Using MSE budgets constructed from the ERA40 and NCEP reanalysis, we tested several mechanisms for a convergence feedback. Tests were inconclusive since in ERA40 (but not in NCEP) low level horizontal advection is comparable to evaporation, so there is not a consistent buildup of column, or even boundary-layer integrated moist static energy that must be vented by deep convection.

It would be interesting to study these mechanisms in a somewhat more idealized situation such as a large-domain CRM simulation, where data assimilation techniques and observational errors would not complicate the analysis. One could also test the “convective initiation” mechanism in this framework. More generally, forays into analyzing column moist static energy budgets have led to further interest in studying the extent to which reanalyses and CRM simulations support current theories about column moist static energy budgets and gross moist stability.

8 Acknowledgements:

This work was supported by NASA grants NAG5-13564 and NAG5-9657. SSM/I, TMI and QuikSCAT datasets are produced by Remote Sensing Systems and sponsored by the NASA Earth Science REASoN DISCOVER Project and NASA Ocean Vector Winds Science Team, respectively. These data are available at www.remss.com from Remote Sensing Systems. The ERA40 reanalysis data was obtained from the DSS at NCAR. The NCEP reanalysis was obtained from the CDC website, <http://www.cdc.noaa.gov>. Dr. Sandra Yuter kindly provided us with echo area fraction time series for the KWAJEX low-PRF radar scans. Discussions with Dave Raymond and Adam Sobel were helpful to the authors in preparing this work.

References

- Arakawa, A., Schubert, W. H. 1974: Interaction of a Cumulus Cloud Ensemble with the Large-Scale Environment, Part I. *J. Atmos. Sci.*, **31**, 674-701.
- Betts, A. K., 1986: A new convective adjustment scheme. Part I: Observational and theoretical basis. *Quart. J. Royal. Meteor. Soc.*, **112**, 677-691.
- Bretherton, C. S., M. E. Peters, and L. E. Back, 2004: Relationships between water vapor path and precipitation over the tropical oceans. *J. Climate*, **17**, 1517-1528
- Houze, R. A., Jr., S. Brodzik, C. Schumacher, S. E. Yuter, and C. R. Williams, 2004:

- Uncertainties in oceanic radar rain maps at Kwajalein and implications for satellite validation. *J. Appl. Meteor.*, **43**, 1114-1132
- Johnson, R. H., and X. Lin, 1997: Episodic trade wind regimes over the western Pacific warm pool. *J. Atmos. Sci.*, **54**, 2020-2034.
- Kalnay, E., and Coauthors, 1996: The NCEP/NCAR 40-Year Reanalysis Project. *Bull. Amer. Meteor. Soc.*, **77**, 437-471.
- Neelin, J. D. and Held, I. M., 1987: Modeling Tropical Convergence Based on the Moist Static Energy Budget. *Mon. Wea. Rev* **115**, 3-12
- Neelin, J. D. and Zeng, N., 2000: A Quasi-Equilibrium Tropical Circulation Model- Formulation. *J. Atmos. Sci.*, **57**, 1741-1766
- Raymond, D. J., 1995: Regulation of moist convection over the west Pacific warm pool. *J. Atmos. Sci.*, **52**, 3945-3959
- Raymond, D. J., G. B. Raga, C. S. Bretherton, J. Molinari, C. Lopez-Carillo and Z. Fuchs, 2003: Convective forcing in the intertropical convergence zone of the east Pacific. *J. Atmos. Sci.*, **60**, 2064-2082
- Sobel, A. H. and C. S. Bretherton, 2000: Modeling tropical precipitation in a single column. *J. Climate*, **13**, 4378-4392
- Sobel, A. H., S. E. Yuter, C. S. Bretherton, and G.N. Kiladis, 2004: Large-scale meteorology and deep convection during TRMM KWAJEX. *Mon. Wea. Rev.*, **132**, 422-444.

Wentz F. J., 1997: A well-calibrated ocean algorithm for SSM/I, *J. Geophys. Res.*, **102**, 8703-8718.

Wentz, Frank J. and Roy W. Spencer, 1998: SSM/I Rain Retrievals within a Unified All-Weather Ocean Algorithm, *J. Atmos. Sci.*, **55**, 1613-1627.

Yuter, S. E., R. A. Houze, Jr., E. A. Smith, T. T. Wilheit, and E. Zipser, 2004: Physical characterization of tropical oceanic convection observed in KWAJEX. *J. Appl. Meteor.*, accepted.

Zebiak, S. E., 1986: Atmospheric Convergence Feedback in a Simple Model for El Nino, *Mon. Wea. Rev.*, **114**, 1263-1271.

List of Figures

- 1 Distribution of daily precipitation binned against wind speed. X's show bin-mean precipitation, and lines show 25th, 50th and 75th percentiles of 60 gridpoint-day bins. 27
- 2 Daily precipitation distribution binned against wind speed for points throughout the Pacific ITCZ, when column relative humidity, r is greater than 0.75. X's show bin-mean precipitation, and lines show 25th, 50th and 75th percentiles of 60 gridpoint-day bins. 28
- 3 QuikSCAT SeaWinds validation of SSM/I wind speed-precipitation relations using data at 95°W , 10°N , for days when $r > 0.75$: (a) daily QuikSCAT vector mean wind speed distribution binned against SSM/I wind speeds, (b) daily precipitation binned against vector mean QuikSCAT wind speed. Plotting conventions are as in previous figures, except bin size is 50 gridpoint-days. 29
- 4 Precipitation-wind speed correlation at different column relative humidities using $5^\circ \times 5^\circ$ SSM/I precipitation and wind speed (top row) as well as QuikSCAT vector mean wind speeds and SSM/I precipitation (bottom 3 panels). Eastern Pacific ($85\text{-}125^\circ\text{W}$, $7.5\text{-}12.5^\circ\text{N}$) mean and quartiles plotted with X's and lines, and Eastern Pacific correlation coefficients shown. Western Pacific ($145\text{-}155^\circ\text{E}$, $2.5^\circ\text{S}\text{-}7.5^\circ\text{N}$) bin means also plotted, as circles. 30

| | | |
|---|---|----|
| 5 | (a) Distribution of daily Kwajalein radar-derived precipitation proxy binned by microwave imager wind speeds from 2 closest 2.5° gridpoints to Kwajalein (bin size: 30 gridpoint-days). (b) same, using SSM/I and TMI precipitation averaged over 2 closest wind speeds. (c) same as a) using QuikSCAT vector mean winds (d) same as b) using QuikSCAT vector mean winds | 31 |
| 6 | Examples of ERA40 and NCEP wind speed-precipitation correlations in eastern and western Pacific at column relative humidity 0.74-0.76 (bin size: 60 gridpoint-days). (a) ERA40 r , precipitation and surface vector mean wind speed used (b) NCEP r , precipitation and surface vector mean wind speed (c) SSM/I-TMI data used. Plotting conventions as in Fig. 4 with only bin means in the east and west Pacific. Correlation coefficients shown for the East Pacific | 32 |
| 7 | Schematic of “vertical MSE advection” mechanism for wind speed-precipitation correlation. Arrows correspond to positive couplings with wind speed, and denote sources and sinks of MSE when (+) or (-) sign is attached. Radiation changes little as wind speed increases. | 33 |
| 8 | Reanalysis column moist static energy (h) advection and surface flux binned as a function of wind speed; advection is separated into vertical and horizontal components. (a) column integrated horizontal h advection. (b) column integrated vertical h advection (associated with convergence in the lower and mid- troposphere and divergence aloft) (c) surface flux. | 34 |

| | | |
|----|---|----|
| 9 | Schematic of “boundary layer quasi-equilibrium” mechanism for wind speed-precipitation correlation. Symbols as in Fig. 7. | 35 |
| 10 | Schematic of “convective initiation” mechanism: evaporation increases shallow cumulus population and column relative humidity modulates percentage of shallow cumulus that deepen into precipitating systems. | 36 |

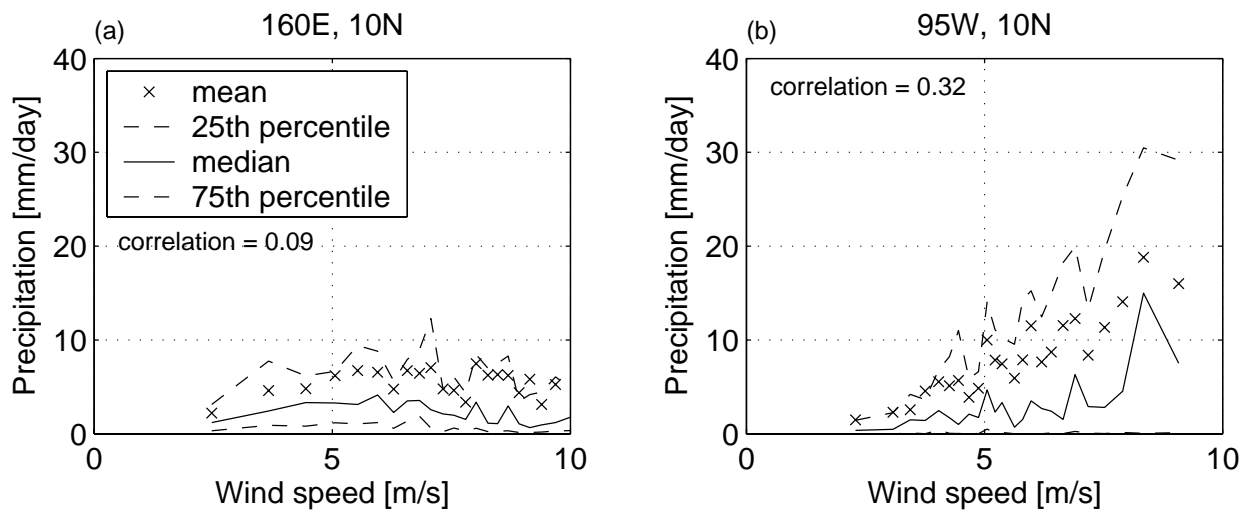


Figure 1: Distribution of daily precipitation binned against wind speed. X's show bin-mean precipitation, and lines show 25th, 50th and 75th percentiles of 60 gridpoint-day bins.

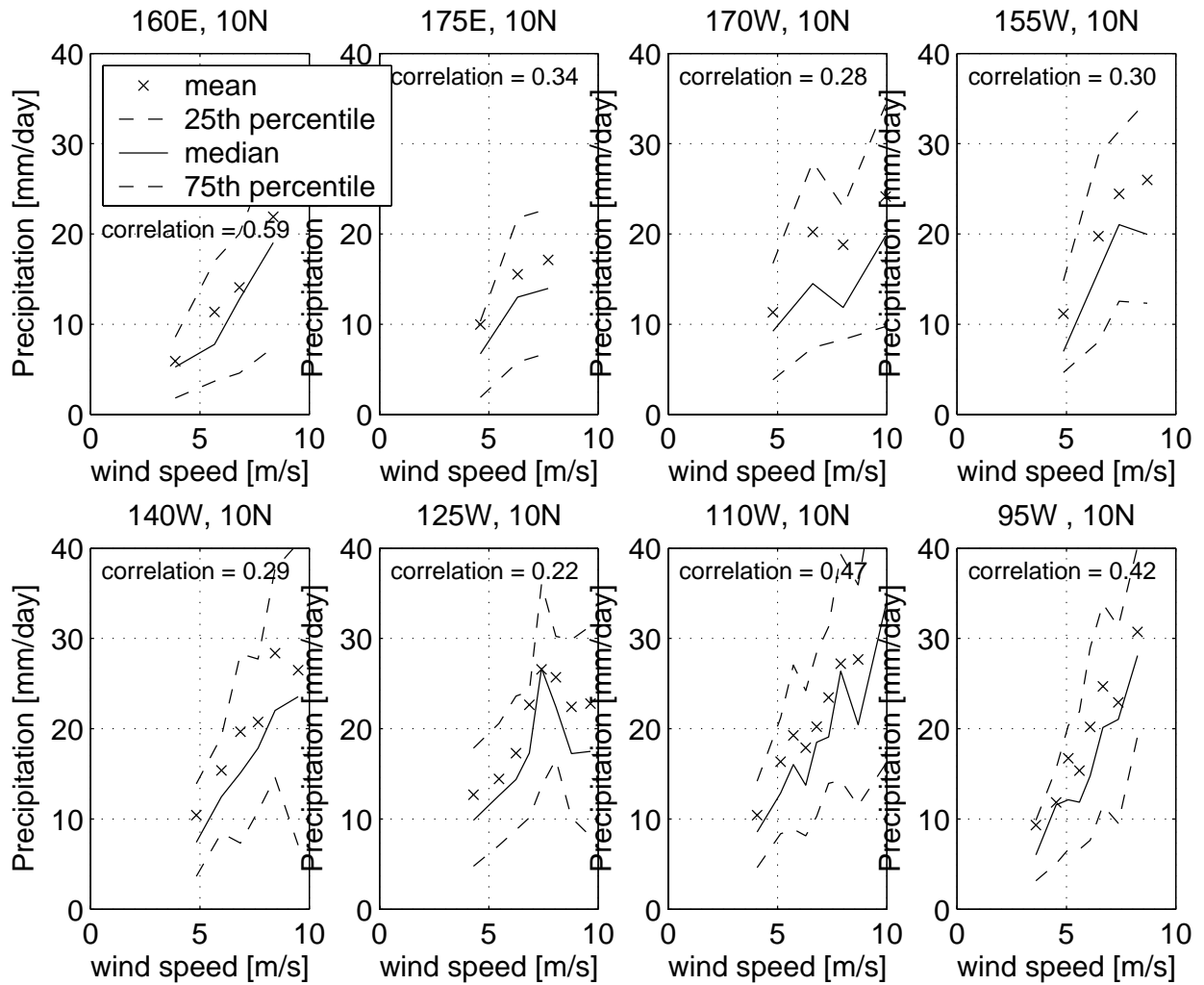


Figure 2: Daily precipitation distribution binned against wind speed for points throughout the Pacific ITCZ, when column relative humidity, r is greater than 0.75. X's show bin-mean precipitation, and lines show 25th, 50th and 75th percentiles of 60 gridpoint-day bins.

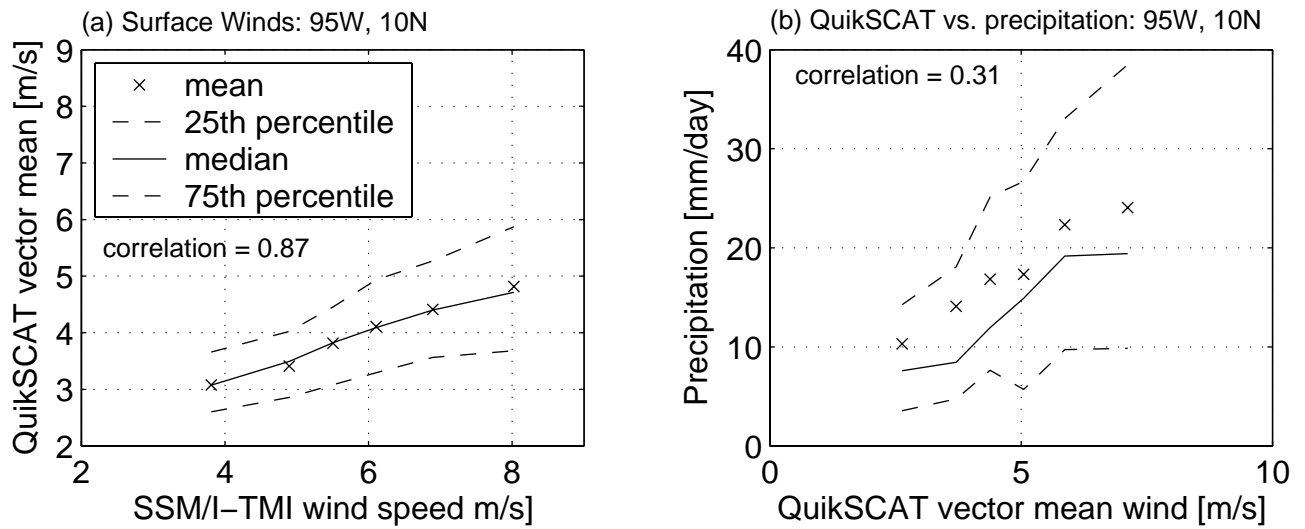


Figure 3: QuikSCAT SeaWinds validation of SSM/I wind speed-precipitation relations using data at 95°W , 10°N , for days when $r > 0.75$: (a) daily QuikSCAT vector mean wind speed distribution binned against SSM/I wind speeds, (b) daily precipitation binned against vector mean QuikSCAT wind speed. Plotting conventions are as in previous figures, except bin size is 50 gridpoint-days.

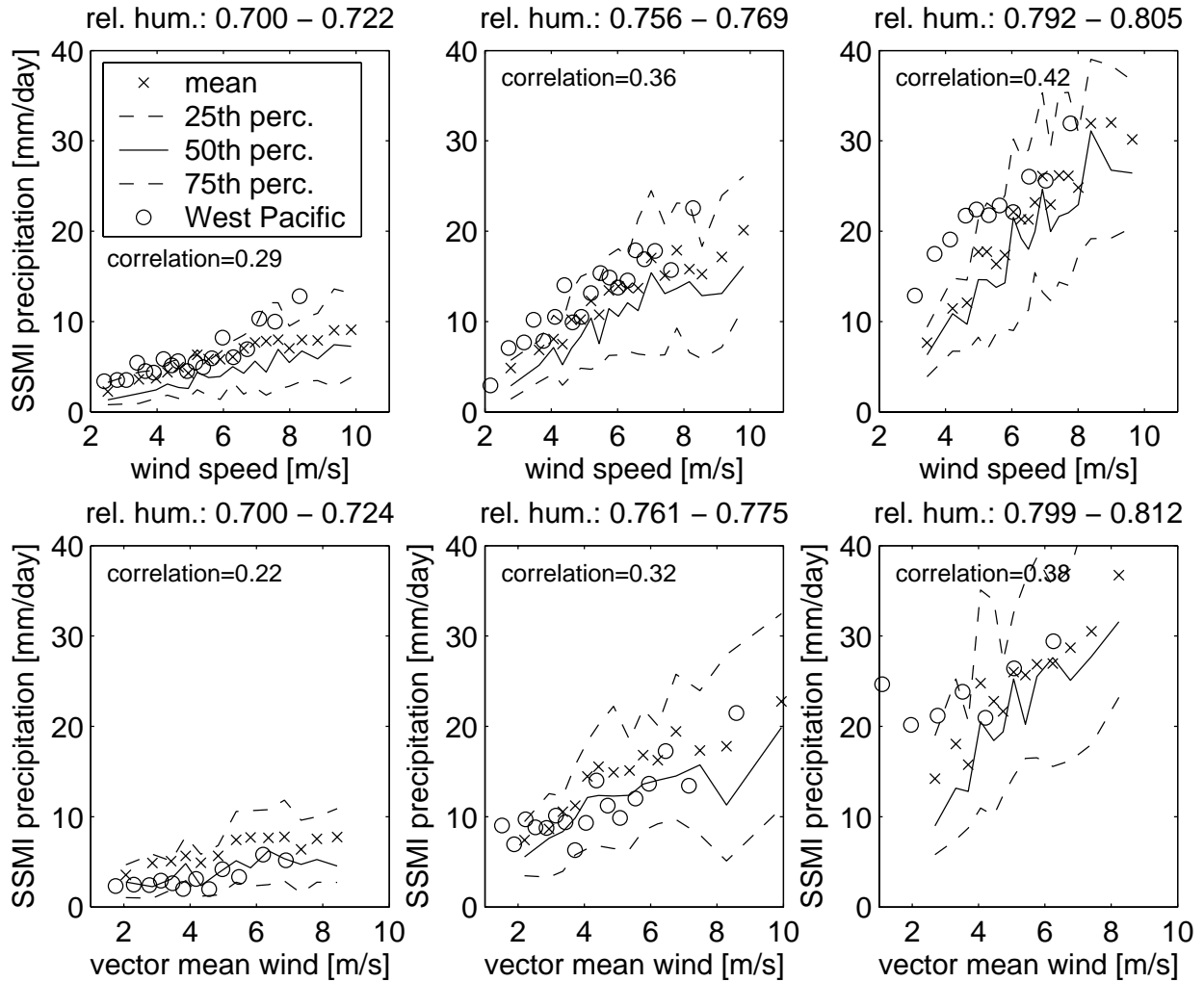


Figure 4: Precipitation-wind speed correlation at different column relative humidities using $5^\circ \times 5^\circ$ SSM/I precipitation and wind speed (top row) as well as QuikSCAT vector mean wind speeds and SSM/I precipitation (bottom 3 panels). Eastern Pacific ($85\text{-}125^\circ\text{W}$, $7.5\text{-}12.5^\circ\text{N}$) mean and quartiles plotted with X's and lines, and Eastern Pacific correlation coefficients shown. Western Pacific ($145\text{-}155^\circ\text{E}$, $2.5^\circ\text{S}\text{-}7.5^\circ\text{N}$) bin means also plotted, as circles.

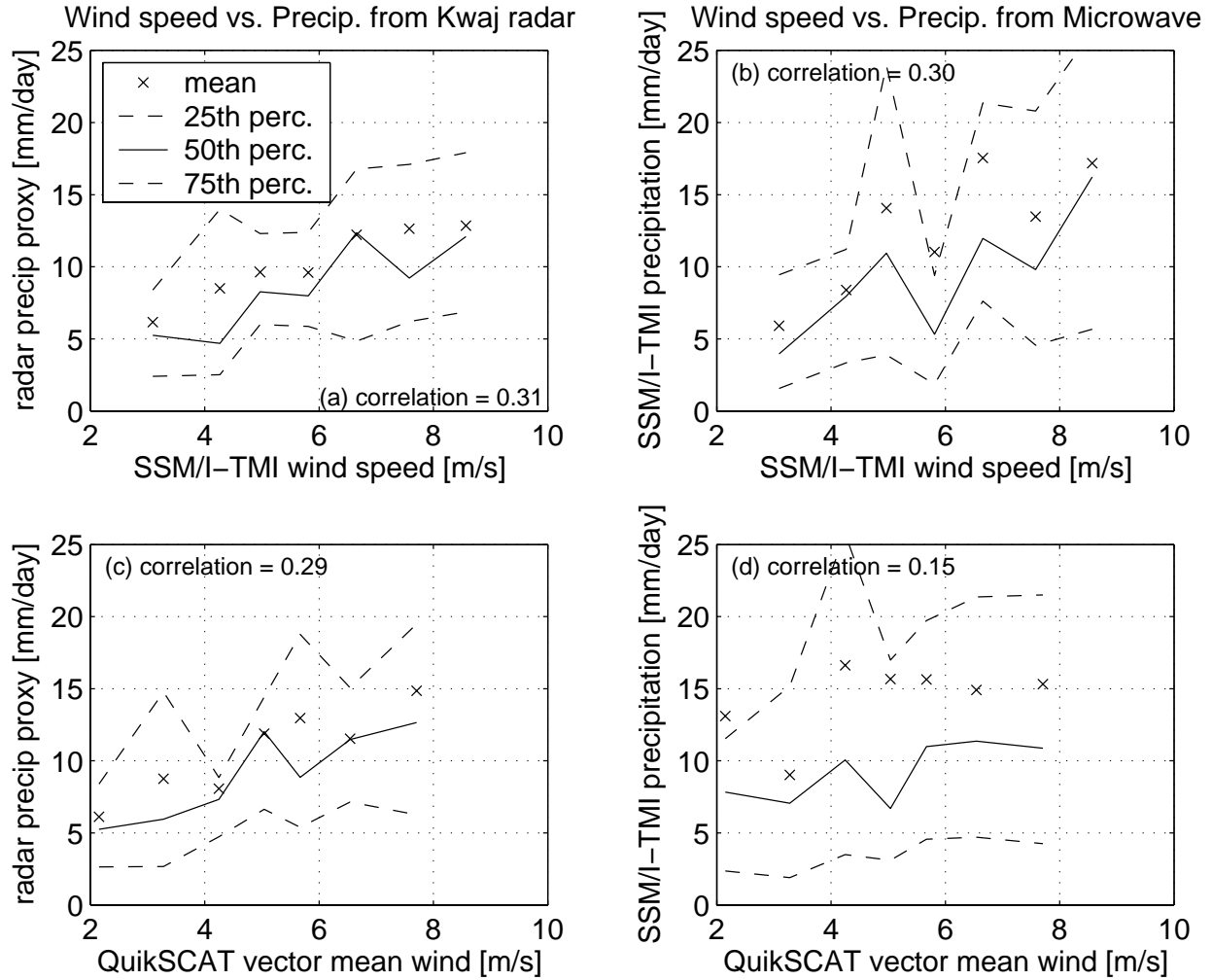


Figure 5: (a) Distribution of daily Kwajalein radar-derived precipitation proxy binned by microwave imager wind speeds from 2 closest 2.5° gridpoints to Kwajalein (bin size: 30 gridpoint-days). (b) same, using SSM/I and TMI precipitation averaged over 2 closest wind speeds. (c) same as a) using QuikSCAT vector mean winds (d) same as b) using QuikSCAT vector mean winds

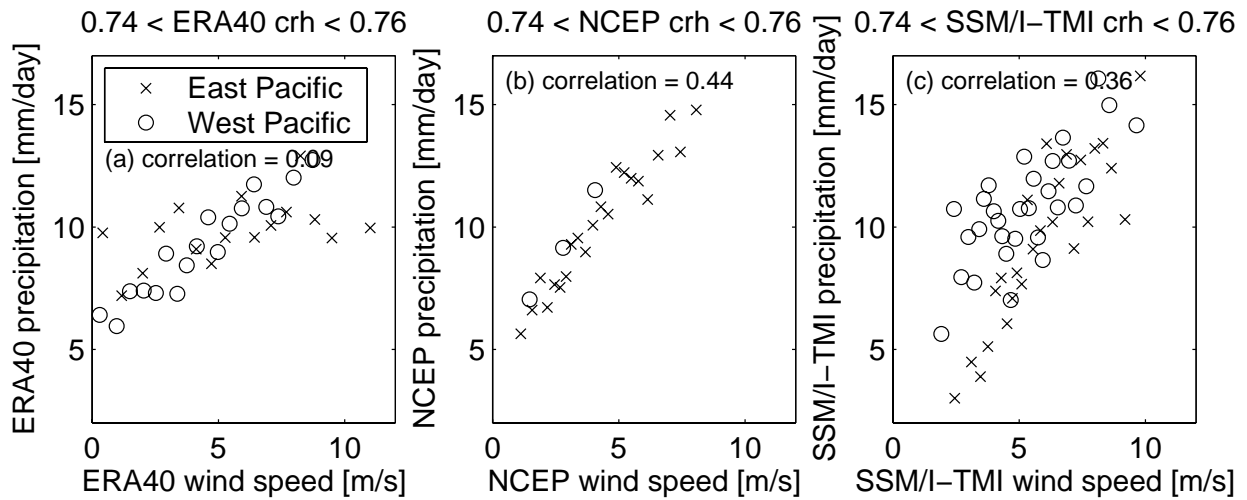


Figure 6: Examples of ERA40 and NCEP wind speed-precipitation correlations in eastern and western Pacific at column relative humidity 0.74-0.76 (bin size: 60 gridpoint-days). (a) ERA40 r , precipitation and surface vector mean wind speed used (b) NCEP r , precipitation and surface vector mean wind speed (c) SSM/I-TMI data used. Plotting conventions as in Fig. 4 with only bin means in the east and west Pacific. Correlation coefficients shown for the East Pacific

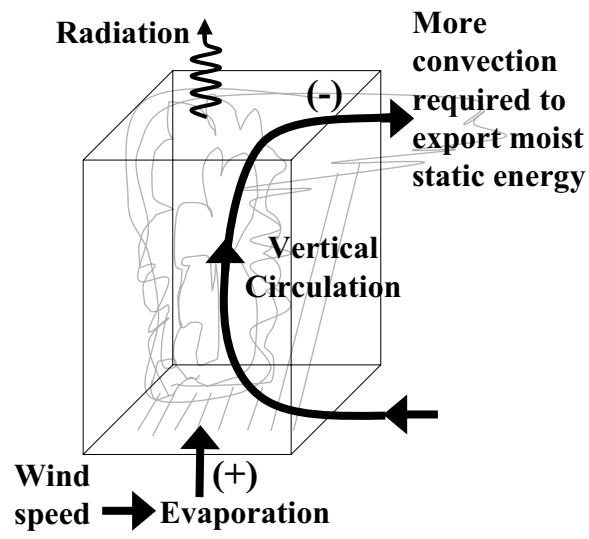


Figure 7: Schematic of “vertical MSE advection” mechanism for wind speed-precipitation correlation. Arrows correspond to positive couplings with wind speed, and denote sources and sinks of MSE when (+) or (-) sign is attached. Radiation changes little as wind speed increases.

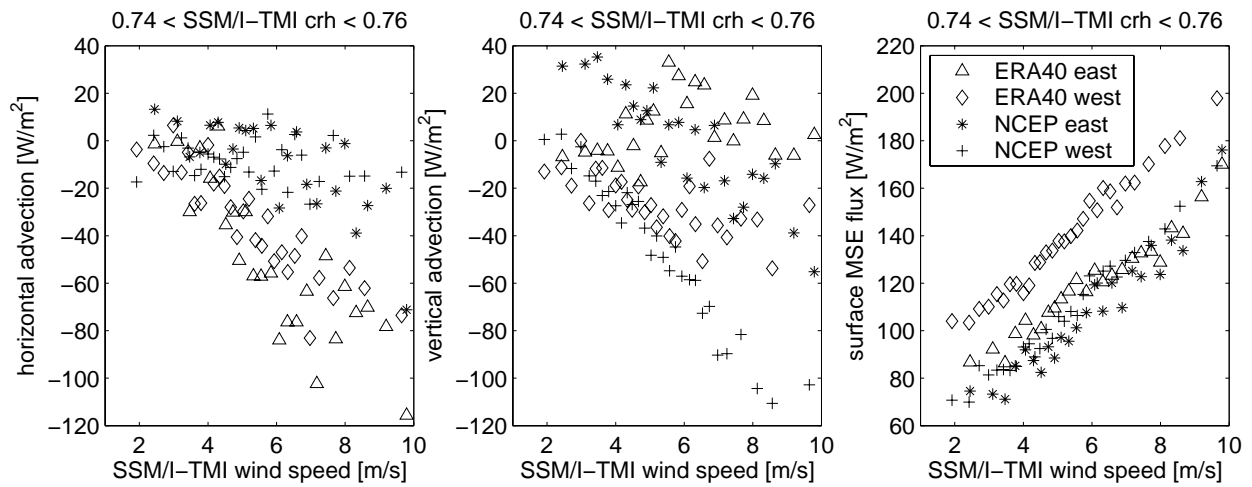


Figure 8: Reanalysis column moist static energy (h) advection and surface flux binned as a function of wind speed; advection is separated into vertical and horizontal components. (a) column integrated horizontal h advection. (b) column integrated vertical h advection (associated with convergence in the lower and mid- troposphere and divergence aloft) (c) surface flux.

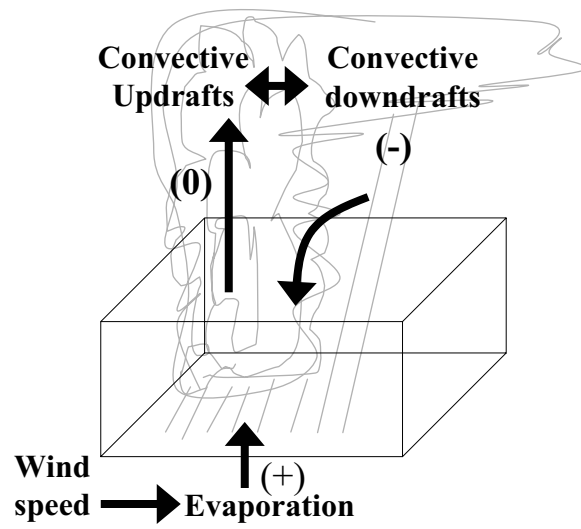


Figure 9: Schematic of “boundary layer quasi-equilibrium” mechanism for wind speed-precipitation correlation. Symbols as in Fig. 7.

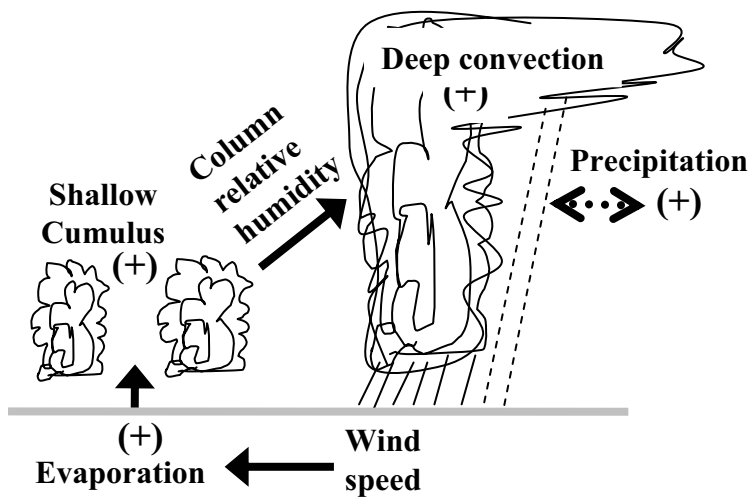


Figure 10: Schematic of “convective initiation” mechanism: evaporation increases shallow cumulus population and column relative humidity modulates percentage of shallow cumulus that deepen into precipitating systems.